Spatio-temporal modeling for regional climate model comparison: application on perennial bioenergy crop impacts

Meng Wang[1], Yiannis Kamarianakis[1],
Matei Georgescu[2,3], Alex Mahalov[1,3,4]
[1]School of Mathematical and Statistical Sciences,
Arizona State University, Tempe, AZ, USA
[2]School of Geographical Sciences and Urban Planning,
Arizona State University, Tempe, AZ, USA
[3]Global Institute of Sustainability, Arizona State University, Tempe, AZ, USA
[4]School of Life Sciences, Arizona State University, Tempe, AZ, USA

Abstract
This article presents spatio-temporal Bayesian models for analyzing regional climate model outputs. WRF simulated temperatures associated with control simulation bias, as well as biofuel impacts, were modeled using three spatio-temporal correlation structures. A hierarchical model with spatially varying intercepts and slopes displayed satisfactory performance in capturing spatio-temporal associations. The effects of microphysics parameterizations in reproducing near-surface climatic conditions were found statistically significant. Simulated temperature impacts due to perennial bioenergy crop expansion were robust to physics parameterization schemes.

Key Words: Bayesian, spatio-temporal, regional climate model, biofuel

1. Introduction

Deployment of perennial bioenergy crops is an alternative energy pathway to mitigate climate change, increase energy independence, stabilize energy prices, and achieve hydroclimatic sustainability in some marginal lands. Previous studies used regional climate models (RCMs) to quantify perennial bioenergy crops impacts [1-5]; however, RCMs with different physics parameterizations could generate significantly different outputs. Therefore, it is essential to assess the significance of factors associated with RCM performance and the robustness of simulated perennial bioenergy crop impacts.

The uncertainties of RCM outputs have been studied using both descriptive and inferential statistics. Specifically, Taylor diagrams and Hövmoller diagrams have been used to evaluate RCM simulation skill using multiple performance metrics [5-7]. However, the abovementioned diagrams cannot be used to assess the significance of factors associated with simulation skill. Sansom et al. (2013) assigned different weights to ensemble members of RCMs, based on an ANOVA framework [8]. This method did not take into account spatiotemporal dependencies. Kang et al. (2012) applied hierarchical Bayesian spatial random-effects models to quantify the climate signal of individual RCMs [9]. Although spatially correlated processes could be captured, the proposed framework did not include a temporal component. Given that spatio-temporal dependencies are inherent to RCM outputs spatio-temporal statistical models are needed.

There is a variety of hierarchical Bayesian spatio-temporal models and corresponding R packages, such as spBayes, spTDyn, spate, spTimer, CARBayesST, and INLA [10-16]. For these models, alternative methods for estimating the posterior distribution have been used, such as Markov chain Monte Carlo (MCMC) sampling [17], and Integrated nested Laplace approximations (INLA) [16]. To our knowledge, a limited number of research works compare alternative parameter estimation approaches and models with different spatio-temporal autocorrelation structures. In this study, multiple spatio-temporal models are compared for modeling regional climate model outputs; the motivating application aims to evaluate perennial bioenergy crop impacts. More specifically, the manuscript investigates the following research questions:

a. Do physics parameterizations and observations have a significant impact on WRF control simulations?

b. Is WRF-simulated temperature impact associated with perennial bioenergy crops robust to alternative physics parameterizations?

c. Which spatio-temporal residual correlation structure is the most appropriate given the fixed effects?

The manuscript is arranged as follows. Section 2 presents a review of Bayesian spatio-temporal models and the methodology of modeling RCM output ensembles. The application is presented and discussed in Section 3. Concluding remarks and suggestions for future work are discussed in Section 4.

2 Spatio-temporal modeling for regional climate model comparison

2.1 Preliminaries

Bayesian hierarchical models possess a 3-stage hierarchical structure: data model, process model and parameters model, i.e.,

(a) Data model, $p(data|process, parameters) = p(Y(s,t)|\mu(s,t), \boldsymbol{\theta})$

(b) Process model, $p(process|parameters) = p(\mu(s,t)|\boldsymbol{\theta})$ and

(c) Parameters model, $p(parameters) = p(\boldsymbol{\theta})$

$\boldsymbol{\theta}$ represents the unknown model parameters, $\mu(s,t)$ is an unknown hidden process, and $Y(s,t)$ refers to the observed data (i.e., RCM outputs in this study). The posterior distribution of the unknown parameters given the observed data is proportional to the product of the three processes. Specifically, the posterior distribution is

$$p(\mu(s,t), \boldsymbol{\theta}|Y(s,t)) \propto p(Y(s,t)|\mu(s,t), \boldsymbol{\theta})\, p(\mu(s,t)|\boldsymbol{\theta})\, p(\boldsymbol{\theta})$$

Typically, such posterior distributions cannot be computed directly; alternative methods of approximation include Markov chain Monte Carlo (MCMC) sampling, and Integrated nested Laplace approximations (INLA).

2.2. WRF model

Simulations were conducted using Weather Research and Forecasting model (WRF, one particular RCM) (Skamarock et al. 2008). WRF is a non-hydrostatic model that solves the nonlinear fully compressible atmospheric equations of motion, coupled to the Noah land surface model (Noah-LSM) [18, 19]. This coupling provides the capability to study the interaction of perennial bioenergy crop-induced land use change and examine hydroclimatic responses to vegetation forcing [19].

The analyzed data are seasonally averaged WRF-simulated temperatures from 2000 to 2009 over the conterminous U.S. Two types of datasets were analyzed (Table 1). The first type relates to simulation bias, i.e., the difference of reproduced temperature and the corresponding observations. Sixteen scenarios were included in this group: scenarios vary by choices of microphysics schemes, cumulus schemes, utility of spectral nudging, and observations. Each of the aforementioned factors includes two levels. The second type of dataset relates to biofuel impact: the difference of reproduced temperature and temperature under full-deployment scenario of perennial bioenergy crops expansion. In the second data type, only two scenarios are included, varied by combinations of physics parameterizations for best and worst skilled model, selected based on a previous study [5]. Further details with regard to the experimental design can be found in [5]. Both types of datasets are gridded data with spatio-temporal dependence. In this study, the datasets were resampled to include 348 pixels at each time period, with 40 time periods in total (seasonal values in consecutive 10 years).

Table 1: Description of datasets

Type of dataset	*Scenarios*	*Microphysics*	*Cumulus physics*	*Spectral nudging technique*	*Observed data*
simulation bias	S1	WSM3	Kain–Fritsch	No	DW
	S2	WSM3	Kain–Fritsch	Yes	DW
	S3	WSM3	Grell 3D	No	DW
	S4	WSM3	Grell 3D	Yes	DW
	S5	WDM6	Kain–Fritsch	No	DW
	S6	WDM6	Kain–Fritsch	Yes	DW
	S7	WDM6	Grell 3D	No	DW
	S8	WDM6	Grell 3D	Yes	DW
	S9	WSM3	Kain–Fritsch	No	GC
	S10	WSM3	Kain–Fritsch	Yes	GC
	S11	WSM3	Grell 3D	No	GC
	S12	WSM3	Grell 3D	Yes	GC
	S13	WDM6	Kain–Fritsch	No	GC
	S14	WDM6	Kain–Fritsch	Yes	GC
	S15	WDM6	Grell 3D	No	GC
	S16	WDM6	Grell 3D	Yes	GC
biofuel impact	S1	WSM3	Kain–Fritsch	No	N/A
	S8	WDM6	Grell 3D	Yes	N/A

2.3. Spatio-temporal statistical modeling

2.3.1 Scenario-specific spatio-temporal models

2.3.1.1 Data model

For each scenario, we considered the following data model:

$$Y(s,t) = \mu(s,t) + \varepsilon(s,t), \text{for } s = 1,\dots,348,\ t = 1,\dots,40, \quad (1)$$

where s represents the areal index, t is the time index, $\mu(s,t)$ represents the mean process, and $\varepsilon(s,t)$ represents noise which is assumed independent (and Gaussian) in space and time:

$$\varepsilon(s,t) \sim Gau\left(0,\ \nu^2\right).$$

2.3.1.2 Process model

RCM outputs were modelled using the following specification:

$$\mu(s,t) = \mu_{.} + a_i + \psi_{s,t}, \text{ for } i = 1, 2, 3, 4 \quad (2)$$

In (2), $\mu_{.}$ represents the overall mean of temperature differences; a_i is a (fixed) seasonal effect (e.g., i =1, 2, 3, and 4 indicates winter, spring, summer and fall respectively, with $\sum_{i=1}^{4} a_i = 0$) while $\psi_{s,t}$ represents the spatio-temporal random effect.

For $\psi_{s,t}$, three structures were evaluated: spatially varying linear time trends with spatially varying intercepts (i.e., STLINEAR, [20]), spatial and temporal main effects and a spatio-temporal interaction (i.e., STANOVA, [21]), and spatio-temporal autoregressive processes (i.e., STAR, [22]).

STLINEAR estimates spatially varying linear trends for each areal unit:

$$\psi_{s,t} = \beta + \phi_s + (\alpha + \delta_s)^* \frac{(t\text{-}\bar{t}\,)}{N},$$
$$\phi_s|\phi_{\text{-}s}, \boldsymbol{W} \sim N\left(\frac{\rho_{int}\sum_{j=1}^{348} w_{sj}\phi_j}{\rho_{int}\sum_{j=1}^{K} w_{sj}+1\text{-}\rho_{int}},\ \frac{\tau_{int}^2}{\rho_{int}\sum_{j=1}^{348} w_{kj}+1\text{-}\rho_{int}}\right), \quad (3)$$
$$\delta_s|\delta_{\text{-}s}, \boldsymbol{W} \sim N\left(\frac{\rho_{slo}\sum_{j=1}^{348} w_{sj}\delta_j}{\rho_{slo}\sum_{j=1}^{348} w_{sj}+1\text{-}\rho_{slo}},\ \frac{\tau_{slo}^2}{\rho_{slo}\sum_{j=1}^{348} w_{sj}+1\text{-}\rho_{slo}}\right),$$

where $\boldsymbol{W} = (w_{sj})$ is a matrix that captures neighborhood relationships between areal units (k_s, k_j).

STANOVA consists of 3 components of spatio-temporal variation: an overall spatial effect common to all time periods ϕ_s, an overall temporal trend common to all spatial units δ_t, and independent space-time interactions $\gamma_{s,t}$. The model is formulated as:

$$\psi_{s,t} = \phi_s + \delta_t + \gamma_{s,t}$$
$$\phi_s|\boldsymbol{\phi_{\text{-}s}}, \boldsymbol{W} \sim N\left(\frac{\rho_S\sum_{j=1}^{348} w_{sj}\phi_j}{\rho_S\sum_{j=1}^{348} w_{sj}+1\text{-}\rho_S},\ \frac{\tau_S^2}{\rho_S\sum_{j=1}^{348} w_{sj}+1\text{-}\rho_S}\right), \quad (4)$$
$$\delta_t|\boldsymbol{\delta_{\text{-}t}}, \boldsymbol{D} \sim N\left(\frac{\rho_T\sum_{j=1}^{40} d_{tj}\delta_j}{\rho_T\sum_{j=1}^{40} d_{tj}+1\text{-}\rho_T},\ \frac{\tau_T^2}{\rho_T\sum_{j=1}^{40} d_{tj}+1\text{-}\rho_T}\right),$$
$$\gamma_{s,t} \sim N(0, \tau_I^2),$$

where $\boldsymbol{W} = (w_{kj})$ is the same as in *(3)*; $\boldsymbol{D} = (d_{tj})$ the temporal neighborhood matrix with $d_{tj} = 1$ if $|j\text{-}t| = 1$ and $d_{tj} = 0$ otherwise.

STAR models the spatio-temporal structure as a multivariate first order autoregressive process with a spatially correlated precision matrix. The model specification is given by:

$$\psi_{s,t} = \phi_{s,t},$$
$$\boldsymbol{\phi_t}|\boldsymbol{\phi_{t-1}} \sim N(\rho_T\phi_{t\text{-}1}, \tau^2\boldsymbol{Q}(\boldsymbol{W}, \rho_S)^{-1}),\ t = 2, \ldots, 40, \quad (5)$$
$$\boldsymbol{\phi_1} \sim N(0, \tau^2\boldsymbol{Q}(\boldsymbol{W}, \rho_S)^{-1}),$$

where $\boldsymbol{\phi_t} = (\phi_{1t}, \ldots, \phi_{40\,t})$, *and* $\boldsymbol{Q}(\boldsymbol{W}, \rho_S) = \rho_S[diag(\boldsymbol{W1})\text{ - }\boldsymbol{W}] + (1 - \rho_S)\boldsymbol{I}$, $\mathbf{1}$ is the 348×1 vector of ones and $\boldsymbol{I}$ is the 348×348 identity matrix.

3.3.1.3 Parameter model

Here we specify the prior distribution for the fixed effects coefficients in *(2)* and the spatio-temporal random effects. Specifically, $\mu_{.}, a_2\text{-}a_1, a_3\text{-}a_1, and\ a_4\text{-}a_1$ in *(2)* were given noninformative priors (i.e., they were distributed in Normal with mean zero and variance 1000). For STLINEAR, the priors were specified as follows:

$\tau_{int}^2, \tau_{slo}^2 \sim Inverse\text{-}Gamma(a, b)$ (random effects variances),
$\rho_{int}, \rho_{slo} \sim Uniform(0,1)$ (spatial dependence parameters), *(6)*
$\alpha \sim N(\mu_\alpha, \sigma_\alpha^2)$ (overall slope parameter),

where the hyperparameters are $(a, b, \mu_\alpha, \sigma_\alpha^2) = (1, 0.01, 0, 1000)$.

For STANOVA,
$\tau_S^2, \tau_T^2, \tau_I^2 \sim Inverse\text{-}Gamma(a, b)$ (random effects variances), *(7)*
$\rho_S, \rho_T \sim Uniform(0,1)$ (spatial/temporal dependent parameter),
where the hyperparameters are $(a, b) = (1, 0.01)$.

For STAR,
$\tau^2 \sim Inverse\text{-}Gamma(a, b)$,
$\rho_S, \rho_T \sim Uniform(0,1)$ (spatial/temporal autoregressive parameter), *(8)*
where the hyperparameters are $(a, b) = (1, 0.01)$.

Posterior samples of spatial and temporal dependence parameters for each model and each scenario were compared using box-plots. The model that had consistent spatio-temporal structure across scenarios was applied on the pooled data (combined scenarios), in order to assess the significance of factors associated with RCM performance and the robustness of estimated perennial bioenergy crop impacts.

2.3.2 Scenario-combined spatio-temporal modeling

We assumed that all scenarios of the same datatype have a consistent spatio-temporal structure: this structure was selected based on the results of scenario-specific models. Scenario-combined models were different from scenario-specific models only with regard to the fixed effects part. For simulation bias, datasets were modelled using the following specification:

$$\mu_{i,j,k,l,m}(s,t) = \mu_{\dots\dots}(s,t) + a_i + b_j + c_k + d_l + e_m + ab_{i,j} + ac_{i,k} + ad_{i,l} + ae_{i,m} + bc_{j,k} + bd_{j,l} + be_{j,m} + cd_{k,l} + ce_{k,m} + de_{l,m} + \psi_{s,t},$$

for $i = 1,2,3,4$, $j = 1,2$, $k = 1,2$, $l = 1,2$, and $m = 1,2$, *(9)*
restricted with $\sum_i a_i = 0$, $\sum_j b_j = 0$, $\sum_k c_k = 0$, $\sum_l d_l = 0$, $\sum_m e_m = 0$,
$\sum_i \sum_j ab_{i,j} = 0$, $\sum_i \sum_k ac_{i,k} = 0$, $\sum_i \sum_l ad_{i,l} = 0$, $\sum_i \sum_m ae_{i,m} = 0$,
$\sum_j \sum_k bc_{j,k} = 0$, $\sum_j \sum_l bd_{j,l} = 0$, $\sum_j \sum_m be_{j,m} = 0$, $\sum_k \sum_l cd_{k,l} = 0$,
$\sum_k \sum_m ce_{k,m} = 0$, and $\sum_l \sum_m de_{l,m} = 0$

Similar to *(2)*, $\mu_{\dots\dots}(s,t)$ represents the overall mean of temperature differences, while $\psi_{s,t}$ denotes the spatio-temporal random effects. a_i, b_j, c_k, d_l, e_m denote fixed effects for seasons, microphysics parameterizations, cumulus scheme parameterizations, spectral nudging and observations, respectively. In addition, $ab_{i,j}, ac_{i,k}, ad_{i,l}, ae_{i,m}, ae_{i,m}, bc_{j,k}, bd_{j,l}, be_{j,m}, cd_{k,l}, ce_{k,m}$, and $de_{l,m}$ represent the corresponding interaction effects.

For biofuel impact, datasets were modelled using the following specification:

$$\mu_{i,j,k,l,m}(s,t) = \mu_{\dots\dots}(s,t) + a_i + b_j + ab_{i,j} + \psi_{s,t},$$

for $i = 1,2,3,4, j = 1,2$, *(10)*
restricted with $\sum_i a_i = 0$, $\sum_j b_j = 0$, and $\sum_i \sum_j ab_{i,j} = 0$

The components are the same as *(9)*, except that b_j represents physics parameterization combinations, and $ab_{i,j}$ the corresponding interaction.

3. Results

3.1 Model comparison using DIC

Model fit for different datasets was evaluated using DIC (Table 2). For all scenarios of simulation bias data-type, STAR achieved the lowest DIC consistently, while STLINEAR attained higher DIC than STANOVA in all scenarios except S5, S6, S8 and S14. On the contrary, STAR models achieved the highest DIC and STLINEAR the lowest for biofuel impact data-type. Thus, STLINEAR fitted the simulation bias data-type worse than the other two spatio-temporal structures, whereas it fitted the biofuel impact data-type better than the other structures. STAR, on the other hand, fitted the simulation bias data-type better, but achieved the worst performance for biofuel impact data-type.

Table 2: DIC of scenario-specific modeling

Type of dataset	*scenario*	*STLINEAR*	*STANOVA*	*STAR*
Simulation bias	S1	30556.8	30299.61	27239.83
	S2	29659.08	29469.15	26759.66
	S3	30323.23	30067.83	26602.55
	S4	29607.56	29502.47	26718.72
	S5	29185.82	28949.95	26354.89
	S6	27905.07	27948.96	26548.55
	S7	29028.95	28669.41	26214.85
	S8	28002.11	28040.67	27057.49
	S9	30610.51	30308.43	27032.93
	S10	29696.17	29525.09	27066.27
	S11	30288.61	30054.88	26887.28
	S12	29586.9	29494.1	26848.38
	S13	29120.41	28823.15	26502.2
	S14	27803.51	27841.85	26549.3
	S15	29221.08	28876.18	26213.22
	S16	27715.63	27701.42	26467.08
Biofuel impact	S1	39255.33	39354.91	39368.12
	S2	38915.38	39041.54	39098.31

3.2 Spatio-temporal modeling of individual scenarios

3.2.1 Fixed effect estimates

The medians of fixed effects were very close across spatio-temporal models; on the other hand, the 95% confidence intervals (CIs) differed dramatically. For example, the estimated medians of simulation biases based on scenario S1 (Table 3) were equal to 2.20, 0.46, 3.51, and 2.75 for the intercept, spring-winter difference, summer-winter difference, and fall-winter difference, respectively. The widest 95% CIs, however, were observed using STAR, whereas the narrowest using STLINEAR. It is worth noting that there were no significant differences for fixed effect estimates derived from alternative approximation methods (i.e., MCMC vs INLA) as the corresponding 95% CIs were overlaid. Results showed that simulated temperature biases differ significantly by season. This finding is consistent across 3 models.

Table 3: Fixed effect estimations of scenario S1 of simulation bias data-type.

Fixed effect	*Model*	*95% Confidence Interval*								
		STLINEAR			*STANOVA*			*STAR*		
		Median	*2.50%*	*97.50%*	*Median*	*2.50%*	*97.50%*	*Median*	*2.50%*	*97.50%*
(Intercept)	MCMC	-2.2	-2.26	-2.14	-2.21	-2.38	-2.05	-2.21	-2.49	-1.95
	INLA	-2.13	-2.21	-2.06	-2.21	-2.4	-2.01			
season2-1	MCMC	0.46	0.38	0.54	0.47	0.2	0.72	0.47	-0.01	0.91
	INLA	0.46	0.37	0.54	0.46	0.19	0.73			
season3-1	MCMC	3.51	3.44	3.59	3.53	3.27	3.82	3.52	3.09	3.99
	INLA	3.51	3.43	3.59	3.52	3.25	3.79			
season4-1	MCMC	2.75	2.67	2.84	2.77	2.53	3.01	2.78	2.36	3.26
	INLA	2.75	2.67	2.84	2.77	2.5	3.04			

3.2.2 Spatio-temporal correlation random effects

For STLINEAR, the range of spatial intercepts and slopes overlaid consistently across scenarios (Figure 1). When modeling simulation bias, the means of spatially dependent intercepts lie between 0.9 and 0.95 whereas the majority of means of spatially dependent slopes range from 0.8 to 0.9 (Figure 1(a) and 1(b)). The spatially dependent variances of slopes differed, with larger magnitudes across scenarios relative to the ones that correspond to intercepts (Figure 1(c) and 1(d)). The overall spatial intercepts were generally greater than 0 for all scenarios (Figure 1(e)). For biofuel impacts, however, the differences of posterior samples across scenarios were relatively small.

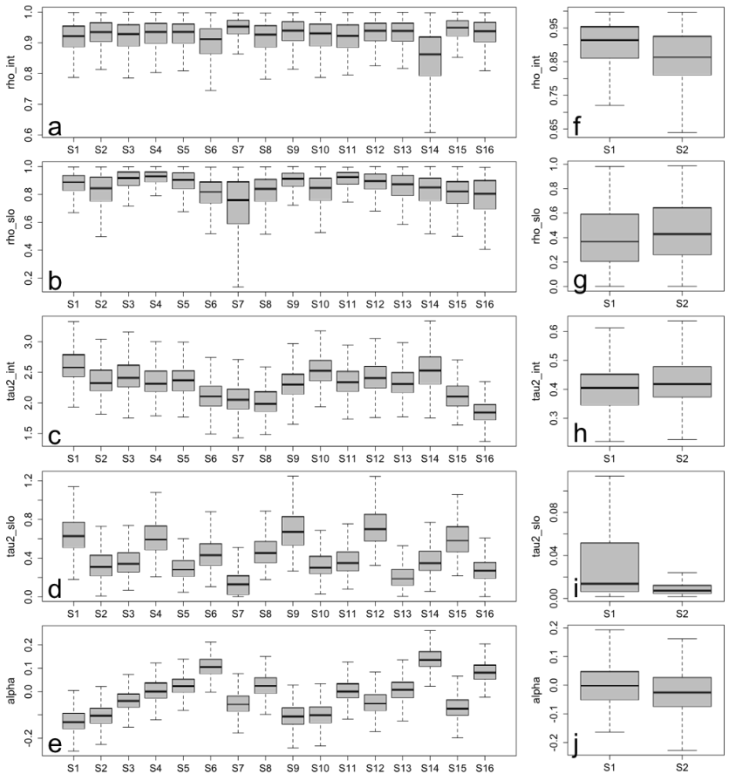

Figure 1: Box-plots of posterior samples of spatio-temporal random effects using STLINEAR. Each box plot corresponds to one scenario-specific model: (a) mean of spatially dependent intercept, associated with simulation bias data-type; (b)-(e) the same as (a) but for mean of spatially dependent slope, variance of spatially dependent intercept, variance of spatially dependent slope, and overall slope parameter, respectively; (f)-(g) the same as (a)-(e), but associated with biofuel impact data-type.

For STANOVA model, although the posterior distributions of spatially dependent means were similar across scenarios, the rest of posterior samples differed dramatically (Figure 2(a)-(e)). Specifically, temporally dependent means, temporally dependent variances, and spatio-temporal interaction terms for simulation bias data had significantly different posterior distributions across scenarios. However, posterior distributions related to biofuel impacts did not differ dramatically, similar to what was observed for STLINEAR.

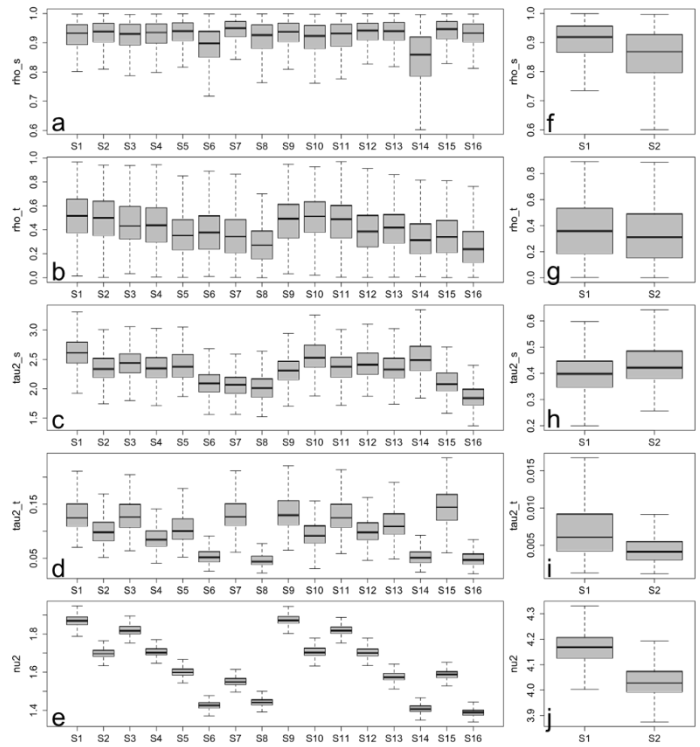

Figure 2: Box-plots of posterior samples of spatio-temporal random effects using STANOVA. Each box plot corresponds to one scenario-specific model: (a) spatially dependent mean, associated with simulation bias data-type; (b)-(e) the same as (a) but for temporally dependent mean, spatially dependent variance, temporally dependent variance, and spatio-temporal interaction, respectively; (f)-(g) the same as (a)-(e), but associated with biofuel impact data-type.

Posterior samples of STAR differed largely across scenarios for both simulation bias and biofuel impact data types (Figure 3). Specifically, posterior samples of temporally autoregressive parameters and variances of spatial autocorrelations could differ on the order of five to seven times across scenarios (Figure 3(b) and 3(c)).

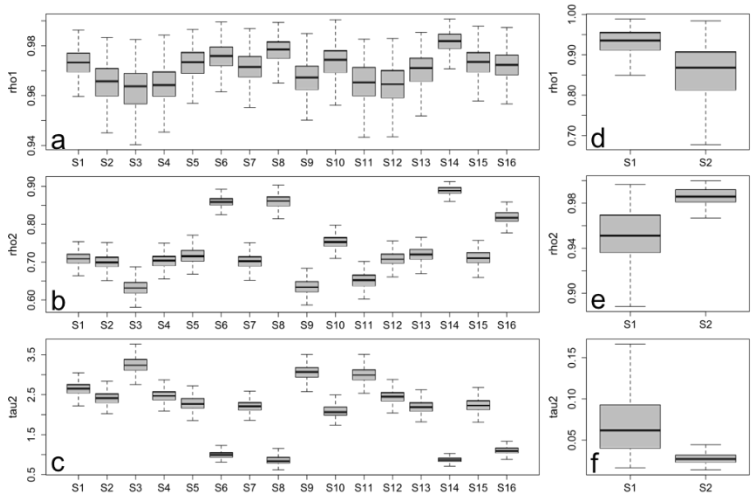

Figure 3: Box-plots of posterior samples of spatio-temporal random effects using STAR. Each box plot corresponds to one scenario-specific model: (a) spatially autoregressive parameters, associated with simulation bias data-type; (b)-(c) the same as (a) but for temporally autoregressive parameters, and variances of spatial autocorrelations, respectively; (d)-(f) the same as (a)-(c), but associated with biofuel impact data-type.

Taking into account the model comparisons presented above and the interest of combining scenarios in a single specification, STLINEAR appears to be the best choice: a consistent spatial-temporal structure can be assumed across scenarios using STLINEAR structure, given that seasonal factors are included.

3.3 Spatio-temporal modeling for scenario-combined data using STLINEAR

3.3.1. Simulation bias

By modeling the scenario-combined data using STLINEAR, the significance of seasons, observations, physics parameterizations, as well as their interactions was examined. It was found that seasons, choices of microphysics, and their interactions have significant impact on simulation bias. On the other hand, choices of cumulus schemes, spectral nudging and observations do not affect the simulation bias. Table 4 presents the outcome of the model building procedure, after statistically non-significant terms were excluded. Summer, fall, and spring have positive impacts on simulation bias with decreasing effects according to the aforementioned order, relative to winter (which corresponds to the intercept in Table 4). A simple ANOVA model would incorrectly characterize spectral nudging and cumulus scheme parameterizations as statistically significant factors for simulation bias (results omitted for brevity).

Table 4: Parameter estimation for scenario-combined simulation bias data-type using STLINEAR. The significant factors are highlighted in bold.

	Median	2.50%	97.50%
(Intercept)	**-2.4849**	**-2.5062**	**-2.4633**
factor(season_dummy)2	**0.4939**	**0.463**	**0.5219**
factor(season_dummy)3	**2.9305**	**2.901**	**2.9588**
factor(season_dummy)4	**2.4143**	**2.3853**	**2.4401**
factor(mc_dummy)1	**1.5358**	**1.508**	**1.5636**
factor(season_dummy)2:factor(mc_dummy)1	**-0.8253**	**-0.8681**	**-0.7929**
factor(season_dummy)3:factor(mc_dummy)1	**-1.4062**	**-1.4495**	**-1.3685**
factor(season_dummy)4:factor(mc_dummy)1	**-1.0666**	**-1.1048**	**-1.0252**
alpha	-0.021	-0.0469	0.0084
tau2.int	2.3822	2.1148	2.7644
tau2.slo	0.8934	0.7465	1.1037
nu2	1.7657	1.7528	1.7786
rho.int	0.9542	0.8712	0.9932
rho.slo	0.8515	0.6835	0.9562

3.3.2 Biofuel impacts

Similarly, the significance of factors associated with biofuel impacts were examined by modeling scenario-combined data. Seasonal effects on biofuel impacts were found statistically significant (Table 5). However, biofuel impacts did not differ significantly for alternative physics parameterizations of WRF. Table 5 depicts the final model which has the lowest DIC among the examined specifications.

Table 5: Parameter estimation for scenario-combined biofuel impact data-type using STLINEAR. The significant factors are highlighted in bold.

	Median	*2.50%*	*97.50%*
(Intercept)	-0.0489	-0.121	0.021
factor(season_dummy)2	**-0.1858**	**-0.2712**	**-0.0965**
factor(season_dummy)3	**-1.6871**	**-1.7777**	**-1.6035**
factor(season_dummy)4	**-0.3193**	**-0.4038**	**-0.2264**
factor(physics_dummy)2	-0.0532	-0.1163	0.0181
alpha	0.0338	-0.0677	0.1397
tau2.int	0.4665	0.3557	0.6026
tau2.slo	0.0072	0.0022	0.0499
nu2	4.5685	4.4825	4.6605
rho.int	0.9194	0.8017	0.9868
rho.slo	0.3819	0.0209	0.9207

4. Concluding remarks

In this study, WRF simulated temperatures associated with control simulation bias, as well as biofuel impacts, were modeled using spatio-temporal bayesian hierarchical models. Our findings suggest that models with spatially varying intercepts and slopes can offer a satisfactory description of the spatio-temporal dependence structure of the data. Microphysics parameterizations have statistically significant impacts on reproducing near-surface climatic conditions. Simulated impacts on temperatures due to perennial bioenergy crop expansion were found robust to physics parameterizations.

This work has several limitations. One of them is that sensitivity analysis of prior distributions was not performed: different prior specifications may result in different inferences. Besides, parameter estimation techniques (i.e., MCMC vs INLA) were not compared in depth. A more through comparison of estimation accuracy and computation times should be considered. In addition, issues related to change of support and alignment were ignored at the pre-processing data stage.

It is worth noting that the physics parameterizations and observations were included in the models as fixed effects under the assumption of spatial and temporal homogeneity. However, it is possible that spatially varying effects exist (Kang et al. 2012). Moreover, multivariate hierarchical spatio-temporal modeling (i.e., for temperature and precipitation simultaneously) should be performed as the aforementioned variables are both significant for model comparison. Despite the above-mentioned limitations, this work established a framework to quantitatively assess the impact of physics parameterizations and observations on WRF simulation, focusing on an application associated with perennial bioenergy crops expansion.

Acknowledgements

The datasets for this study were generated for a project funded by NSF grant EAR-1204774.

References

[1] Anderson, C. J., Anex, R. P., Arritt, R. W., Gelder, B. K., Khanal, S., Herzmann, D. E., & Gassman, P. W. (2013). Regional climate impacts of a biofuels policy projection. *Geophysical Research Letters*, *40*(6), 1217-1222.

[2] Georgescu, M., Lobell, D. B., & Field, C. B. (2011). Direct climate effects of perennial bioenergy crops in the United States. *Proceedings of the National Academy of Sciences*, *108*(11), 4307-4312.

[3] Khanal, S., Anex, R. P., Anderson, C. J., Herzmann, D. E., & Jha, M. K. (2013). Implications of biofuel policy-driven land cover change for rainfall erosivity and soil erosion in the United States. *GCB Bioenergy*, *5*(6), 713-722.

[4] Wagner, M., Wang, M., Miguez-Macho, G., Miller, J., VanLoocke, A., Bagley, J. E., Bernacchi, C. J. and Georgescu, M. (2016). A realistic meteorological assessment of perennial biofuel crop deployment: A southern Great Plains perspective. *GCB Bioenergy*, In Press, doi:10.1111/gcbb.12403

[5] Wang, M., Wagner, M., Miguez-Macho, G., Kamarianakis, Y., Mahalov, A., Moustaoui, M., …, & Georgescu, M. (2016). On the long-term hydroclimatic sustainability of perennial bioenergy crop expansion over the United States. *Journal of Climate.* Manuscript submitted for publication.

[6] Hovmöller, E. (1949). The Trough-and-Ridge diagram. *Tellus*, *1*(2), 62-66.

[7] Taylor, K. E. (2001). Summarizing multiple aspects of model performance in a single diagram. *Journal of Geophysical Research: Atmospheres*, *106*(D7), 7183-7192.

[8] Sansom, P. G., Stephenson, D. B., Ferro, C. A., Zappa, G., & Shaffrey, L. (2013). Simple uncertainty frameworks for selecting weighting schemes and interpreting multimodel ensemble climate change experiments. *Journal of Climate*, *26*(12), 4017-4037.

[9] Kang, E. L., Cressie, N., & Sain, S. R. (2012). Combining outputs from the North American regional climate change assessment program by using a Bayesian hierarchical model. *Journal of the Royal Statistical Society: Series C (Applied Statistics)*, *61*(2), 291-313.

[10] Finley, A. O., Banerjee, S., & Carlin, B. P. (2013). spBayes: Univariate and multivariate spatial modeling. *R package version 0.3-8, URL http://cran. r-project. org/web/packages/spBayes*.

[11] Bakar, K. S., Kokic, P., & Jin, H. (2016). Hierarchical spatially varying coefficient and temporal dynamic process models using spTDyn. *Journal of Statistical Computation and Simulation*, *86*(4), 820-840.

[12] Sigrist, F., Künsch, H. R., & Stahel, W. A. (2015). spate: an R package for statistical modeling with SPDE based spatio-temporal Gaussian processes.

[13] Sigrist, F., Künsch, H. R., & Stahel, W. A. (2012). A dynamic nonstationary spatio-temporal model for short term prediction of precipitation. *The Annals of Applied Statistics*, 1452-1477.

[14] Bakar, K. S., & Sahu, S. K. (2015). sptimer: Spatio-temporal bayesian modelling using r. *Journal of Statistical Software*, *63*(15), 1-32.

[15] Lee, D., Rushworth, A., & Napier G. Spatio-Temporal Areal Unit Modelling in R with Conditional Autoregressive Priors Using the CARBayesST Package.

[16] Blangiardo, M., & Cameletti, M. (2015). *Spatial and Spatio-temporal Bayesian Models with R - INLA*. Wiley.

[17] Gilks, W. R., Richardson, S. and Spiegelhalter, D. J. (eds) (1996) Markov Chain Monte Carlo in Practice. London: Chapman and Hall.

[18] Chen, F., & Dudhia, J. (2001). Coupling an advanced land surface-hydrology model with the Penn State-NCAR MM5 modeling system. Part I: Model implementation and sensitivity. *Monthly Weather Review*, *129*(4), 569-585.

[19] Ek, M. B., Mitchell, K. E., Lin, Y., Rogers, E., Grunmann, P., Koren, V., ... & Tarpley, J. D. (2003). Implementation of Noah land surface model advances in the National Centers for Environmental Prediction operational mesoscale Eta model. *Journal of Geophysical Research: Atmospheres*, *108*(D22).

[20] Bernardinelli, L., Clayton, D., Pascutto, C., Montomoli, C., Ghislandi, M., & Songini, M. (1995). Bayesian analysis of space—time variation in disease risk. *Statistics in medicine*, *14*(21-22), 2433-2443.

[21] Knorr-Held, L. (1999). Bayesian modelling of inseparable space-time variation in disease risk. Institute of Statistics, LMU Munich.

[22] Rushworth, A., Lee, D., & Mitchell, R. (2014). A spatio-temporal model for estimating the long-term effects of air pollution on respiratory hospital admissions in Greater London. *Spatial and spatio-temporal epidemiology*, *10*, 29-38.